Synthesis and Oxygen Reduction Activity of Shape-Controlled Pt3Ni Nanopolyhedra. Nano Letters 10 (2):638-644

ARTICLE *in* NANO LETTERS · FEBRUARY 2010

Impact Factor: 13.59 · DOI: 10.1021/nl903717z · Source: PubMed

4 AUTHORS, INCLUDING:

Hongzhou Yang
Miami University
26 PUBLICATIONS **999** CITATIONS
SEE PROFILE

Shouzhong Zou
American University Washington D.C.
74 PUBLICATIONS **2,409** CITATIONS
SEE PROFILE

NANO LETTERS

pubs.acs.org/NanoLett

Synthesis and Oxygen Reduction Activity of Shape-Controlled Pt_3Ni Nanopolyhedra

Jun Zhang,[†] Hongzhou Yang,[‡] Jiye Fang,*[,†] and Shouzhong Zou*[,‡]

[†]Department of Chemistry, State University of New York at Binghamton, Binghamton, New York 13902 and
[‡]Department of Chemistry and Biochemistry, Miami University, Oxford, Ohio 45056

ABSTRACT Platinum-based alloys have been extensively shown to be effective catalysts for oxygen reduction reaction (ORR) in proton exchange membrane fuel cells (PEMFCs). Most of these catalysts are nanoparticles without shape control. Recently, extended $Pt_3Ni(111)$ surfaces prepared in ultrahigh vacuum were demonstrated to possess enhanced ORR catalytic activity as compared to the state-of-the-art carbon supported Pt (Pt/C) nanoparticle catalysts. How and whether this promising surface can be transformed into practical nanoscale electrocatalysts used in PEMFCs remain a challenge. We report a new wet-chemical approach of preparing monodisperse Pt_3Ni nanoctahedra and nanocubes terminated with {111} and {100} facets, respectively. We further show that the ORR activity on the Pt_3Ni nanoctahedra is ~5-fold higher than that of nanocubes with a similar size. Comparison of ORR activity between carbon-supported Pt_3Ni nanoctahedra and commercial Pt/C reveals that the Pt_3Ni nanoctahedra are highly active electrocatalysts. This synthetic strategy may be extended to the preparation of other shape-controlled fuel cell electrocatalysts.

KEYWORDS Pt_3Ni, oxygen reduction activity, tungston hexacarbonyl, nanoctahedron, nanocube

It is an urgent task to seek other energetic resources or different energy conversion pathways to replace the burning of fossil fuels such as gasoline or diesel, due to the increasing worldwide energy demand and environmental concerns. One of the promising efforts is the development of fuel cell technology. Fuel cells exhibit exciting performance advantages for power generation by converting the chemical energy of a fuel directly into electricity. The intense interest in fuel cell technology stems from the fact that fuel cells are environmentally benign and extremely efficient. Among various types of fuel cells, the proton-exchange membrane fuel cells (PEMFCs) and direct methanol fuel cells (DMFCs) are appealing for automotive and portable electronic applications owing to their low operation temperatures.[1−3] Both PEMFCs and DMFCs use polymer electrolyte membrane (PEM) and platinum (Pt)[4,5] or Pt-based alloys catalysts. Unfortunately, the slow rate of the oxygen-reduction reaction (ORR), the high cost, and the vulnerability toward reaction poisons of Pt electrocatalyst remain serious limitations to many applications.[3,6] In this regard, it is crucial for fuel cell development to explore more active and poison-resistant catalysts that are superior to the traditionally employed carbon-supported platinum (Pt/C) particle systems. There has been considerable progress on the search for Pt-based bimetallic electrocatalysts, such as forming Pt−Pd nanocomposites,[7,8] or Pt-monolayer on a second metal,[9] or alloying Pt with less expensive 3d-transition metals,[10,11] including Fe,[11,12] Co,[13,14] Ni,[15,16] Cu,[17,18] Cr,[12] and Mn.[15] It was reported that the catalytic activity of Pt_3M (M = V, Ti, Co, Fe, Ni) is significantly improved[19,20] with strong resistance to poisonous substances.[21] Recently, Stamenkovic et al. demonstrated that extended single crystal surfaces of $Pt_3Ni(111)$ exhibit an enhanced ORR activity that is 10-fold higher than Pt(111) and 90-fold higher than the current state-of-the-art Pt/C catalysts.[22] Such a remarkable activity was attributed to the weaker OH adsorption arising from the decrease of the d-band center on the Pt skin formed by surface segregation. Like many other heterogeneous catalysis studies,[23,24] a fundamental question is whether such a high activity observed on the extended single crystal surfaces can be obtained from nanometer-sized particles. To bridge this size gap, the challenge is to produce crystal facet-controlled monodisperse {111}-bounded Pt_3Ni nanocrystals (NCs). Although Monte Carlo simulation suggested that {111}-facet-terminated Pt_3Ni nanoctahedra would be energetically stable and have a surface segregation profile similar to that of the extended Pt_3Ni surfaces,[22,25] direct experimental evidence has not been obtained. Herein, we report our synthesis of monodisperse Pt_3Ni nanoctahedra and nanocubes, which are enclosed by {111} and {100} facets, respectively, via a high-temperature organic solution chemistry approach. We demonstrate that the ORR activity on Pt_3Ni nanoctahedra is significantly higher than that on Pt_3Ni nanocubes.

Experimental Section. ***Chemicals and Materials.*** Tungsten hexacarbonyl ($W(CO)_6$, 97%), oleic acid (90%), and oleylamine (70%) are Aldrich products and were used as received. Platinum(II) acetylacetonate ($Pt(acac)_2$, 49.3−49.8% Pt), nickel(II) acetylacetonate ($Ni(acac)_2$, 97%), anhydrous ethanol (200 proof), and anhydrous hexane (98.5%) were from Gelest, Alfa Aesar, AAPER, and BDH, respectively, without further purification. Nickel(II) chloride hexahydrate

* To whom correspondence should be addressed: jfang@binghamton.edu (J. F. for synthesis/structure); zous@muohio.edu (S. Z. for electrochemistry).
Received for review: 11/6/2009
Published on Web: 01/15/2010

DOI: 10.1021/nl903717z | *Nano Lett.* **2010,** *10,* 638-644

(96+%) was received from Fisher Scientific. Commercial Pt/C catalyst (HiSpec 4000, 40 wt % Pt) was purchased from Alfa Aesar. Carbon black (Vulcan XC-72) was received from Carbot corporation, Billerica, MA.

Synthesis of Pt_3Ni Nanoctahedra and Nanocubes. A typical procedure for synthesizing Pt_3Ni nanoctahedra is as follows: Under airless condition, $Pt(acac)_2$ (20 mg, 0.05 mmol), $Ni(acac)_2$ (10 mg, 0.04 mmol), oleylamine (9.0 mL), and oleic acid (1.0 mL) were loaded into a three-neck flask and heated to 130 °C under an argon stream. Tungsten hexacarbonyl ($W(CO)_6$, 50 mg, 0.14 mmol) was then added into the vigorously stirred solution, and the temperature was subsequently raised to 230 °C and allowed to remain there for 40 min with vigorous agitation. The resultant products were isolated by centrifugation after adding a sufficient amount of absolute ethanol and washed with anhydrous hexane for several cycles. The Pt_3Ni nanooctahedra were finally redispersed in hexane, forming a colloidal suspension. The yield was estimated as high as ~80% on the basis of Pt. To synthesize Pt_3Ni nanocubes, $Pt(acac)_2$ (20 mg, 0.05 mmol), oleylamine (9.0 mL), and oleic acid (1.0 mL) were similarly loaded into a three-neck flask under an argon stream. Once the system was heated to 130 °C, $W(CO)_6$ (50 mg, 0.14 mmol) was then added into the vigorously stirred solution. Subsequently, a stock solution of Ni-precursors (0.4 mL, 0.04 mmol), which was preprepared by dissolving 0.238 g of nickel(II) chloride hexahydrate into a mixed solvents containing oleylamine (5.0 mL) and oleic acid (5.0 mL), was added dropwise within 15 min while the temperature was steadily raised from 130 to 200 °C. The colloids were further evolved at 240 °C for an additional 15 min. The isolation procedure of these Pt_3Ni nanocubes is the same as that for Pt_3Ni nanoctahedra. The Pt-based yield of Pt_3Ni nanocubes was estimated as ~70%.

Synthesis of Pt Nanocubes. The procedure was exactly the same as that for Pt_3Ni nanoctahedra, except for the absence of Ni precursors.

Structural Analysis. X-ray diffraction (XRD) patterns were collected using a PANalytical X'Pert X-ray powder diffractometer equipped with a Cu $K\alpha_1$ radiation source ($\lambda = 0.15406$ nm). A Hitachi 7000 transmission electron microscope (TEM) operated at 110 kV was used for traditional TEM imaging and a JEOL-2010 FEG TEM operated at 200 kV was used for high-resolution transmission electron microscopy (TEM) imaging, selected-area electron diffraction, and energy-dispersive X-ray spectroscopy (EDS) data collection. Inductively coupled plasma (ICP) analysis was conducted in Department of Geosciences, University of Houston. Scanning electron micrographs were recorded on a field emission scanning electron microscope (SEM, Carl Zeiss Supra 55 VP).

Electrode Preparation and Electrochemical Measurements. The thin layers of catalysts supported on glassy carbon were prepared by using two methods. For Pt_3Ni NCs, a spin-coating method was applied. In short, glassy carbon disk electrodes (Pine Research Instrumentation, Raleigh, NC, 5 mm diameter) were polished to a mirror-finish prior to each experiment and served as substrates for the catalysts. In each case a thin film of Pt_3Ni NCs on a glassy carbon electrode was formed by spin-coating using a spin coater (Headway Research Inc., Garland, TX) with a drop of Pt_3Ni NC suspension. The Pt_3Ni NC suspension was obtained by washing the as-prepared colloidal suspension twice with hexane to remove the majority of unbound surfactants and then redispersing in hexane. The amount of Pt_3Ni NCs on the glassy carbon can be increased by repeating the spin-coating process. The glassy carbon electrode supported Pt_3Ni NC catalysts were subjected to an argon plasma (100 W, 0.3 Torr) (PX250, March Plasma Systems, Concord, CA) treatment for 5 min to remove the residual organic solvent and surfactants on Pt_3Ni NCs. The electrodes were then subjected to an electrochemical treatment by potential cycling between 0.05 and 1.0 V at 100 mV s^{-1} until stable voltammograms were obtained, typically around 40 cycles. For Pt_3Ni octa/C and Pt/C catalysts, we followed Watanabe's method[26] to prepare the catalyst layer on the glassy carbon electrode. Commercially available Pt/C catalyst (Alfa Aesar, 40 wt % Pt) was used to prepare 0.2 μg of Pt/μL of catalyst suspension. A constant volume (18 μL) of the suspension was pipetted onto a glassy carbon surface and dried under ethanol vapor pressure. A 10 μL portion of 0.05 wt % Nafion solution was then coated on top of the dried catalyst layer and the electrode was dried under ethanol pressure. Electrochemical treatment was similar to that of Pt_3Ni NC catalysts.

The electrochemical experiments were conducted with a CHI 700B electrochemical analyzer (CH instruments, Austin, TX) and a rotating disk assembly (Pine Research Instrumentation, Raleigh, NC) in a two-compartment electrochemical cell. A Pt wire served as the counter electrode, and a Ag/AgCl electrode saturated with KCl was used as the reference electrode. The electrode potential in this study, however, is reported with respect to the RHE. The electrolyte, 0.1 M $HClO_4$, was prepared from double-distilled 70% $HClO_4$ (GFS Chemicals, Columbus, OH) with 18.2 MΩ cm^{-1} water purified by a Milli-Q system (Synthesis A10, Millipore, Billerica, MA). All of the experiments were conducted at room temperature (22 ± 1 °C).

Results and Discussion. It is generally accepted that the development of NCs in a solution system consists of a nucleation stage and a subsequent Ostwald ripening growth on the existing seeds (or nuclei).[27,28] In the rapid nucleation stage, kinetic deposition of atom clusters onto seeds is mainly driven by the supersaturation of the precursors,[29] whereas in the Ostwald ripening growth the NC shape may be thermodynamically controlled by the difference of the surface energy on each crystallographic face.[30] The short nucleation burst often consumes most precursors, resulting in small and less-shape-controlled colloids due to insufficient feedstock for the growth stage. To circumvent this, a dynamic injection approach, in which additional feedstock was continuously provided to the system during the stage of

DOI: 10.1021/nl903717z | *Nano Lett.* **2010,** *10,* 638-644

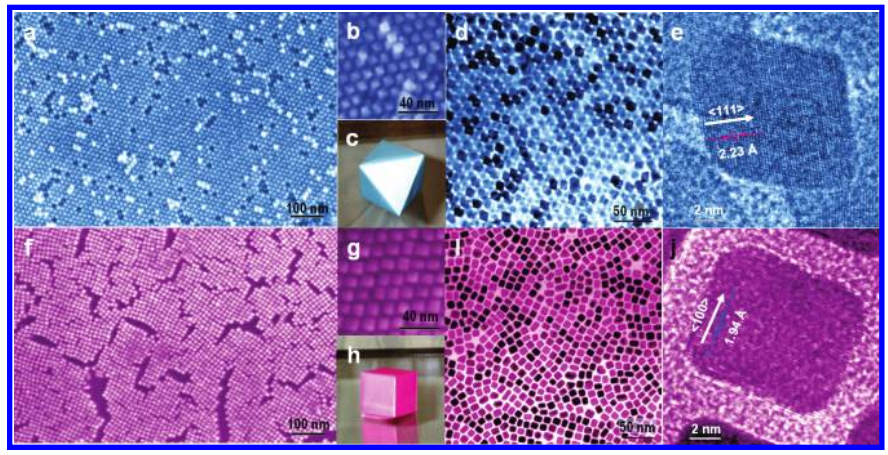

FIGURE 1. (a–e) Images for Pt_3Ni nanoctahedra. (f–j) Images for Pt_3Ni nanocubes. (a, f) Field-emission SEM images. (b, g) High-resolution SEM images. (c) 3D image of an octahedron. (d, i) TEM images. (e, j) High-resolution TEM images of single NCs. (h) 3D image of a cube.

Ostwald ripening growth, was previously employed in preparation of oxide[31,32] and semiconductor[33,34] NCs. Unfortunately, this method was unsuccessful in the synthesis of Pt_3Ni NCs. We therefore instead chose to control the nucleation rate by introducing a foreign element, tungsten (W), to "self-provide" stable sources of Pt clusters in the growth stage. Using this strategy, Pt_3Ni nanoctahedra were successfully prepared via a reaction between $Ni(acac)_2$ and $Pt(acac)_2$ in a mixture of oleic acid and oleylamine at ~200 °C in the presence of $W(CO)_6$ (refer to the Experimental Section). Generally, it is very effective to control the morphology of NCs by introducing foreign metallic ions or a metal in situ decomposed from a carbonyl. For example, Fe and Ag ions have been used to tune the nanostructure of Pt,[35,36] and $Fe(CO)_5$ has also been employed in the particle shape-control of PtFe[37] and Pt[4] NCs. In our preparation, it was revealed that the presence of $W(CO)_6$ is the key in the Pt_3Ni shape control. Without $W(CO)_6$, Pt_3Ni NCs can still be generated, but their morphology appeared much less controlled. Since W does not alloy with Pt under the reaction conditions,[38,39] which is supported by inductively coupled plasma mass spectroscopic (ICP-MS) and EDS analyses,[40] we propose that the relatively low redox-potential of W decomposed from $W(CO)_6$, in comparison with that of Pt,[41] could help reduce $Pt(acac)_2$ to Pt atoms (or seeds) rapidly in the early stage of the reaction, leading to a fast Pt-nucleation,[42,43] whereas the resultant W cations may be accumulated in a relatively high concentration that will decelerate the subsequent metallic particle growth under the following equilibrium ($Pt^{2+} + W^0 \rightleftarrows W^{n+} + Pt^0$). Thus, the Pt/precursor–W system acts as a "buffer", ensuring a steady growth of particles with a sufficient feedstock.[44] A piece of evidence supporting this notion is the observation of a W^{6+} peak in the XPS spectra of the reaction residue. The low rate of Pt-nucleation favors the evolution of Pt_3Ni NCs because Pt clusters can be steadily and continuously provided for the Ostwald growth in this case. In a face-centered cubic system,[28,30] both theoretical prediction[45,46] and experimental investigation[46,47] indicate that Pt_3Ni {111} facets are thermodynamically most stable and have a lowest growth rate in ⟨111⟩ directions. This promotes a rapid elimination of other Pt_3Ni planes,[48,49] leading to the formation of Pt_3Ni nanoctahedra. It is worth mentioning that the combined capping ligands, oleic acid–oleylamine, are indispensable. Not only is oleylamine a reducing agent, but it also plays a role of stabilizing Pt_3Ni {111} by lowering the surface energy on Pt_3Ni {111} facets. Without them, the synthesis of Pt_3Ni nanoctahedra was unsuccessful. Note that facets being more selectively capped by oleic acid–oleylamine are not fixed but rather strongly dependent on the material. For instance, it has been reported that a combination of oleic acid–oleylamine facilitates the stabilization of Pt {100} facets, instead of Pt {111} planes.[50]

By sharing this insight, we further prepared Pt_3Ni nanocubes using the same recipe as that for nanoctahedral synthesis except for a slower rate of injecting nickel chloride hexahydrate into the system in a temperature range between 130 and 200 °C (refer to the Experimental Section).[44] Due to the lack of stoichiometric nickel precursors in this approach, Pt seeds at the initial stage as well as Pt-surface-enriched Pt_3Ni NCs in the subsequent steps should always dominate the crystal growth, which is the driving force for developing cubic NCs. On the other hand, the extremely strong capability for Ni to alloy with Pt enables the limited amount of Ni, reduced from the slowly titrated nickel precursors, to promptly combine with Pt through interlayer diffusions without formation of pristine Ni-phase, or the Pt-core–Ni-shell structure.[51] Our investigation shows that pure Ni NCs could be detected only when the nickel precursors were introduced at a temperature higher than 210 °C.

The shape of these size-selected nanoctahedra was first determined using field-emission scanning electron microscopy (FE-SEM) as shown in Figure 1a. A high-resolution SEM image (Figure 1b, also see Figure S1 in the Supporting Information) further reveals the feature of octahedral surfaces on these NCs (the octahedral model is shown in Figure 1c). Due to the high uniformity in both size and shape, the Pt_3Ni nanoctahedra can be assembled into a multilayered

DOI: 10.1021/nl903717z | *Nano Lett.* **2010,** *10,* 638-644

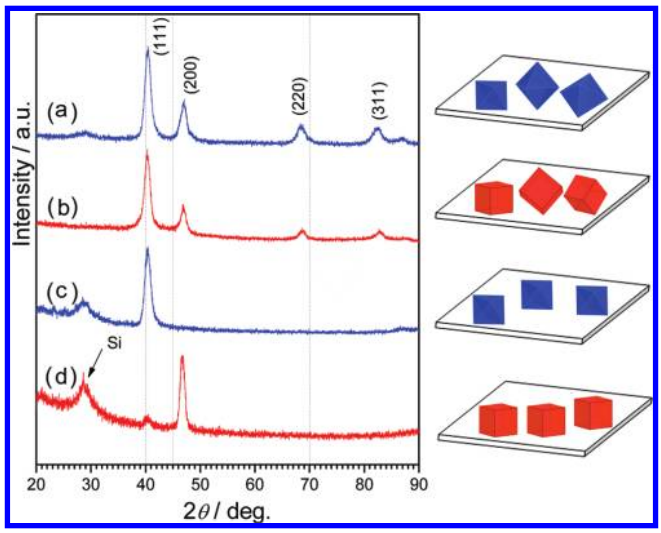

FIGURE 2. XRD pattern of Pt_3Ni NCs. (a, c) Nanoctahedra. (b, d) Nanocubes. (a, b) Samples were randomly deposited on a PANalytical Si Zero background sample holder. (c, d) Samples were assembled on a polished Si wafer.

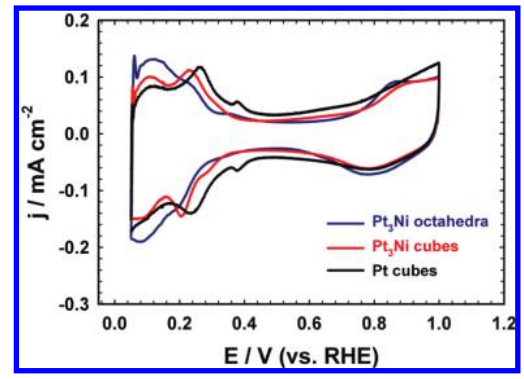

FIGURE 3. Cyclic voltammograms of Pt_3Ni nanoctahedra, Pt_3Ni nanocubes, and Pt nanocubes in 0.1 M $HClO_4$ solution. Scan rate: 100 mV s^{-1}.

superlattice with characteristic dimensions on the order of micrometers. Figure 1d (also see Figure S2 in Supporting Information) presents a TEM image of a multilayer Pt_3Ni pattern, further confirming the octahedral morphology. The arrays of rhombus projection images clearly indicate that all of the octahedral NCs are patterned on the grid (also on the SEM substrate) in [110] projected orientation with an average side length of ~10.6 ± 0.3 nm.[32] Figure 1e (also see Figure S3 in Supporting Information) is a high-resolution TEM (HRTEM) image taken from a projection direction of ⟨110⟩, showing a {111}-*d*-spacing of ~2.23 Å which corresponds well with the lattice spacing of Pt_3Ni ⟨110⟩. No distortion with crystal cores was observed from the HRTEM image. These observations imply that the NCs are dominated by {111}-terminated faces. To further confirm the chemical composition, ICP-MS and EDS analyses (from both TEM and SEM) were conducted, and the results suggest that the average molar ratio between Pt and Ni is 3:1.[40] Figure 1f illustrates an SEM image of Pt_3Ni nanocube monolayer assembly. The pattern is (100)-textured, flat on the top surface and on the order of tens of micrometers. The {100}-perfect orientation can be further verified by the HRSEM (Figure 1g) as well as the XRD pattern (vide infra). As shown in Figure 1h, the projection image of such a cubic model should be a square. Figure 1i demonstrates a typical TEM image of the Pt_3Ni nanocubes. The average side length of these selected nanocubes was measured[52] as ~10.3 ± 0.3 nm. An HRTEM image of a selected Pt_3Ni nanocube (Figure 1j) reveals a highly crystalline cube with clearly resolved lattice fringes with a {200}-*d*-spacing of ~1.94 Å. Composition analyses of this sample show that the average molar ratio of Pt/Ni is 3:1.[40]

To further examine the microstructures of these NCs, XRD patterns were recorded and are presented in Figure 2. When both nanoctahedral (Figure 2a) and nanocubic (Figure 2b) samples were randomly deposited on a PANalytical Si-zero-background sample holder, similar diffraction patterns were obtained, and they are indexed as those of Pt_3Ni based on the previous reports.[53,54] However, assembly of each sample on a surface-polished Si-wafer results in an apparent enhancement on either peak (111) (for nanoctahedra, Figure 2c) or peak (200) (for nanocubes, Figure 2d)[55] and the absence of other peaks. As discussed previously,[37,50,56,57] this observation in macroscale further supports the conclusion from the TEM studies, indicating that nanoctahedra and nanocubes, which are perfectly terminated with {111} and {100} facets, are the dominant shapes in the two samples, respectively.

In order to evaluate their electrocatalytic activities, the NCs were coated on a glassy carbon electrode using a spin-coating method. Before ORR kinetics measurements, these NCs were subjected to potential cycling between 0.05 and 1.0 V (versus a reversible hydrogen electrode, RHE) for ~40 cycles in 0.1 M $HClO_4$ to further clean the particle surface. As shown by Figure S4 in Supporting Information, no obvious change of particle morphology was observed in their TEM projection image after this potential cycling treatment on the Pt_3Ni nanoctahedra. Compared to conventional spherical Pt−Ni NCs without shape control, these NCs are more stable against the leaching of Ni. After more than 40 cycles of CV between 0.05 and 1.0 V, Pt/Ni molar ratio remains unchanged as revealed by the ICP-MS measurements. The resultant final voltammograms are shown in Figure 3. For Pt_3Ni nanoctahedra, the current responses from hydrogen adsorption/desorption processes appear in the potential range of 0.05−0.30 V. The peak position and shape resemble those of the extended Pt_3Ni(111) surface prepared under ultrahigh vacuum (UHV), which is covered with a Pt skin.[22] Similarly, for Pt_3Ni nanocubes, a pair of hydrogen adsorption/desorption peaks at ~0.23 V are close to those observed on the extended Pt_3Ni(100) surface, which is also Pt-rich.[22] On Pt nanocubes (the TEM morphology is displayed in Figure S5 in Supporting Information), two pairs of hydrogen adsorption/desorption peaks at ~0.27 and ~0.37 V, respectively, clearly suggest the dominance of a {100} facet on Pt nanocubes.[58] In addition, the negative shift of the hydrogen

DOI: 10.1021/nl903717z | *Nano Lett.* **2010,** *10,* 638-644

adsorption/desorption peaks on Pt_3Ni nanocubes with respect to those on Pt nanocubes is similar to that on the corresponding extended $Pt_3Ni(100)$ and Pt(100) surfaces.[22] These observations suggest that the NC surfaces are Pt-rich. The presence of a Pt-rich outermost layer is further supported by using surface sensitive carbon monoxide (CO) electro-oxidation, which shows that the CO oxidation peak in the stripping voltammograms obtained on Pt_3Ni nanoctahedra and nanocubes nearly overlaps with that on Pt cubes (Figure S6 in Supporting Information). If there were a significant amount of Ni on the surface, the CO stripping peak would be much more negative than that on the pure Pt.[59] The fidelity of using either hydrogen adsorption/desorption or CO stripping peak positions to confirm the particle surface structure has been extensively shown by others for Pt single crystal surfaces and nanoparticles.[60–63] Monte Carlo simulations[25] suggested that 98% of the outermost layer of Pt_3Ni octahedral NCs contains Pt and nearly 70% of the second layer consists of Ni. Our determination of the Pt-rich particle surface is in agreement with this prediction.

To examine the effect of different crystal facets on the ORR kinetics, rotating disk electrode (RDE) voltammetry was used. The ORR measurements were conducted in an O_2-saturated 0.1 M $HClO_4$ solution at 295 K. A characteristic set of polarization curves for the ORR on Pt_3Ni nanoctahedra, Pt_3Ni nanocubes, and Pt nanocubes are displayed in Figure 4a. Two distinguishable potential regions were clearly observed in the polarization curves: the well-defined diffusion-limiting current region from 0.18 to ~0.7 V and the mixed kinetic-diffusion control region between ~0.8 and 1.0 V. From Figure 4a, it is apparent that the ORR activity is strongly dependent on the particle shape and the composition. After the mass transport correction, the specific activity, that is, the current density with respect to the electrochemically active Pt surface area (ECASA, refer to Table S1 in Supporting Information) at 0.9 V, of Pt_3Ni nanoctahedra is 5.1 times of that of the Pt_3Ni nanocubes and ~6.5 times of that of the Pt nanocubes (Figure 4b). The ECASA was estimated from the charges involved in desorption of the underpotentially deposited hydrogen (H_{UPD}) on the NC surface.[20,64,65] Similarly, the mass activity measured as the current at 0.9 V normalized to the **Pt mass** of the Pt_3Ni nanoctahedra is ~2.8 times of that of Pt_3Ni nanocubes and ~3.6 times of that of Pt nanocubes. The significant shape-dependent ORR activity agrees with the observation from the extended Pt_3Ni single crystal surfaces,[22] where the activity increases in the following order: $Pt_3Ni(100) < Pt_3Ni(110) \ll Pt_3Ni(111)$. Compared with the extended $Pt_3Ni(111)$ and $Pt_3Ni(100)$ surfaces, the specific activity observed on Pt_3Ni nanoctahedra and nanocubes is about 4- to 7-fold smaller, which is in general agreement with the notion that the ORR activity of Pt nanoparticle catalysts is 5 to 10 times smaller than the extended Pt surfaces.[22] The activity improvement of Pt_3Ni nanocubes over Pt nanocubes is small (Figure 4b), which is similar to that of the extended $Pt_3Ni(100)$ and Pt(100) surfaces.[22] To compare their ORR performance with commercially available Pt/C catalysts, the Pt_3Ni nanoctahedra were supported on carbon black (designated as Pt_3Ni-octa/C, Figure S8 in Supporting Information). Their CV in 0.1 M $HClO_4$ and ORR polarization curve are compared with those of Pt/C in Figures S9 and S10 in Supporting Information, respectively. The specific and mass activities of Pt_3Ni-octa/C are ~7 and ~4 times, respectively, higher than those of the commercial Pt/C catalysts (Figure S11 in Supporting Information), though the size of the Pt_3Ni nanoctahedra is ~3 times larger,[66–68] indicating that the Pt_3Ni-octa/C prepared through this new synthesis strategy is a promising electrocatalyst with superior ORR activity and can possibly be used in the cathode of PEMFCs.

Conclusions. Our findings clearly demonstrate that ORR activity strongly depends on the terminal facets of Pt_3Ni NCs. The {111}-facet-terminated nanoctahedra are significantly more active than the {100}-bounded nanocubes, suggesting that controlling the shape of nanocatalyst may be an effective way to improve ORR activity and to develop highly active electrocatalysts used in the real world. The preliminary result from carbon-supported specimens suggests that

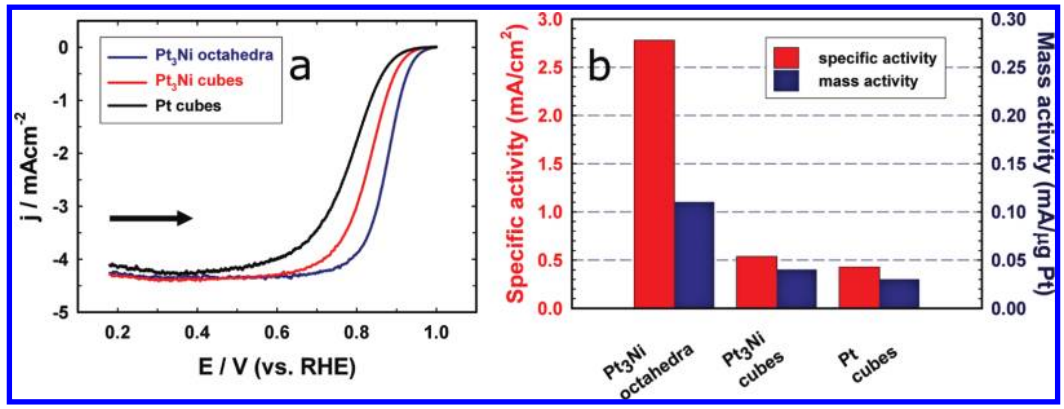

FIGURE 4. (a) Polarization curves for ORR on Pt_3Ni nanoctahedra, Pt_3Ni nanocubes, and Pt nanocubes supported on a rotating GC disk electrode in O_2 saturated 0.1 M $HClO_4$ solution at 295 K; scan rate, 20 mV s^{-1}; rotation rate, 900 rpm. Catalyst loading in terms of Pt mass: Pt_3Ni octahedra, 3.0 μg; Pt_3Ni cube, 2.0 μg; Pt cube, 1.1 μg. Current density was normalized to the glassy carbon geometric surface area (0.196 cm^2). The arrow indicates the potential scan direction. (b) Comparison of the ORR activities on the three types of catalysts. Specific activity and mass activity were all measured at 0.9 V vs RHE at 295 K.

DOI: 10.1021/nl903717z | *Nano Lett.* **2010,** *10,* 638-644

a much higher ORR activity on Pt_3Ni nanoctahedra could be obtained as long as their size can be further decreased. Furthermore, the shape-dependent ORR activity likely exists on other metallic catalysts. The shape-controlled strategy reported herein may be extended to the syntheses of other nonprecious metal−Pt nanopolyhedral alloys, which are candidates of highly active fuel cell catalysts.

Acknowledgment. This work was supported by the NSF (DMR-0731382 and CHM-0616436), the DOE (DE-FG02-07ER86296 and DE-SC0000932), S^3IP, and Binghamton University. Part of the ICP work was done at the University of Houston. We thank A. Kumbhar, Q. Liu, Z. Luo, K. Sun, and I.-T. Bae for their assistance with the TEM/EDS studies.

Supporting Information Available. EM images of Pt_3Ni nanoctahedra, Pt nanocubes, and carbon-supported Pt_3Ni nanoctahedra, CO stripping voltammograms, EDS results, ECASA data, CV curves, and ORR curves/activities of carbon-supported Pt_3Ni nanoctahedra and Pt/C. This material is available free of charge via the Internet at http://pubs.acs.org.

REFERENCES AND NOTES

(1) Dresselhaus, M. S.; Thomas, I. L. *Nature* **2001**, *414*, 332–337.
(2) Winter, M.; Brodd, R. J. *Chem. Rev.* **2004**, *104*, 4245–4270.
(3) Vielstich, W.; Lamm, A.; Gasteiger, H. A. *Handbook of Fuel Cells: Fundamentals, Technology, Applications*; Wiley: New York, 2003.
(4) Wang, C.; Daimon, H.; Onodera, T.; Koda, T.; Sun, S. *Angew. Chem., Int. Ed.* **2008**, *47*, 3588–3591.
(5) Ren, J.; Tilley, R. D. *J. Am. Chem. Soc.* **2007**, *129*, 3287–3291.
(6) Gasteiger, H. A.; Kocha, S. S.; Sompalli, B.; Wagner, F. T. *Appl. Catal., B* **2005**, *56*, 9–35.
(7) Peng, Z.; Yang, H. *J. Am. Chem. Soc.* **2009**, *131*, 7542–7543.
(8) Lim, B.; Jiang, M.; Camargo, P. H. C.; Cho, E. C.; Tao, J.; Lu, X.; Zhu, Y.; Xia, Y. *Science* **2009**, *324*, 1302–1305.
(9) Adzic, R. R.; Zhang, J.; Sasaki, K.; Vukmirovic, M. B.; Shao, M.; Wang, J. X.; Nilekar, A. U.; Mavrikakis, M.; Valerio, J. A.; Uribe, F. *Top. Catal.* **2007**, *46*, 249–262.
(10) Stamenkovic, V.; Mun, B. S.; Mayrhofer, K. J. J.; Ross, P. N.; Markovic, N.; Rossmeisl, J.; Greeley, J.; Nørskov, J. K. *Angew. Chem., Int. Ed.* **2006**, *45*, 2897–2901.
(11) Stamenkovic, V. R.; Mun, B. S.; Arenz, M.; Mayrhofer, K. J. J.; Lucas, C. A.; Wang, G.; Ross, P. N.; Markovic, N. M. *Nat. Mater.* **2007**, *6*, 241–247.
(12) Mukerjee, S.; Srinivasan, S.; Soriaga, M. P. *J. Electrochem. Soc.* **1995**, *142*, 1409–1422.
(13) Watanabe, M.; Tsurumi, K.; Mizukami, T.; Nakamura, T.; Stonehart, P. *J. Electrochem. Soc.* **1994**, *141*, 2659–2668.
(14) Koh, S.; Leisch, J.; Toney, M. F.; Strasser, P. *J. Phys. Chem. C* **2007**, *111*, 3744–3752.
(15) Mukerjee, S.; Srinivasan, S. *J. Electroanal. Chem.* **1993**, *357*, 201–224.
(16) Stamenkovic, V.; Schmidt, T. J.; Ross, P. N.; Markovic, N. M. *J. Electroanal. Chem.* **2003**, *554−555*, 191–199.
(17) Koh, S.; Strasser, P. *J. Am. Chem. Soc.* **2007**, *129*, 12624–12625.
(18) Xu, D.; Liu, Z.; Yang, H.; Liu, Q.; Zhang, J.; Fang, J.; Zou, S.; Sun, K. *Angew. Chem., Int. Ed.* **2009**, *48*, 4217–4221.
(19) Stamenkovic, V.; Schmidt, T. J.; Ross, P. N.; Markovic, N. M. *J. Phys. Chem. B* **2002**, *106*, 11970–11979.
(20) Paulus, U. A.; Wokaun, A.; Scherer, G. G.; Schmidt, T. J.; Stamenkovic, V.; Radmilovic, V.; Markovic, N. M.; Ross, P. N. *J. Phys. Chem. B* **2002**, *106*, 4181–4191.
(21) Serov, A.; Kwak, C. *Appl. Catal., B* **2009**, *90*, 313–320.
(22) Stamenkovic, V. R.; Fowler, B.; Mun, B. S.; Wang, G.; Ross, P. N.; Lucas, C. A.; Markovic, N. M. *Science* **2007**, *315*, 493–497.
(23) Chen, M.; Goodman, W. D. *Chem. Soc. Rev.* **2008**, *37*, 1860–1870.
(24) Somorjai, G. A.; Park, J. Y. *Chem. Soc. Rev.* **2008**, *37*, 2155–2162.
(25) Fowler, B.; Lucas, C. A.; Omer, A.; Wang, G.; Stamenkovic, V. R.; Markovic, N. M. *Electrochem. Acta* **2008**, *53*, 6076–6080.
(26) Higuchi, E.; Uchida, H.; Watanab, M. *J. Electroanal. Chem.* **2005**, *583*, 69–76.
(27) Murray, C. B.; Kagan, C. R.; Bawendi, M. G. *Annu. Rev. Mater. Sci.* **2000**, *30*, 545–610.
(28) Xiong, Y.; Xia, Y. *Adv. Mater.* **2007**, *19*, 3385–3391.
(29) Zhang, J.; Sun, K.; Kumbhar, A.; Fang, J. *J. Phys. Chem. C* **2008**, *112*, 5454–5458.
(30) Wang, Z. L. *J. Phys. Chem. B* **2000**, *104*, 1153–1175.
(31) Liu, Q.; Lu, W.; Ma, A.; Tang, J.; Lin, J.; Fang, J. *J. Am. Chem. Soc.* **2005**, *127*, 5276–5277.
(32) Lu, W.; Liu, Q.; Sun, Z.; He, J.; Ezeolu, C.; Fang, J. *J. Am. Chem. Soc.* **2008**, *130*, 6983–6991.
(33) Qian, C.; Kim, F.; Ma, L.; Tsui, F.; Yang, P.; Liu, J. *J. Am. Chem. Soc.* **2004**, *126*, 1195–1198.
(34) Lu, W.; Gao, P.; Jian, W. B.; Wang, Z. L.; Fang, J. *J. Am. Chem. Soc.* **2004**, *126*, 14816–14821.
(35) Chen, J.; Herricks, T.; Xia, Y. *Angew. Chem., Int. Ed.* **2005**, *44*, 2589–2592.
(36) Song, H.; Kim, F.; Connor, S.; Somorjai, G. A.; Yang, P. *J. Phys. Chem. B* **2005**, *109*, 188–193.
(37) Chen, M.; Kim, J.; Liu, J. P.; Fan, H.; Sun, S. *J. Am. Chem. Soc.* **2006**, *128*, 7132–7133.
(38) Xiong, L.; He, T. *Electrochem. Commun.* **2006**, *8*, 1671–1676.
(39) Alexeev, O.; Shelef, M.; Gates, B. C. *J. Catal.* **1996**, *164*, 1–15.
(40) The compositions of both octahedral and cubic samples were evaluated using ICP-MS, EDS-SEM, and EDS-TEM methods. For nanoctahedra, the average molar ratio of Pt:Ni was determined as 67:33, 70:30, and 76:24 from three methods, respectively. For nanocubes, it was 71:29, 75:25, and 77:23 (Figure S7 in Supporting Information). Content of W was determined as zero from both samples using any of the above methods.
(41) Vanysek, P. In *CRC Handbook of Chemistry and Physics*, 87th ed.; Lide, D. R., Ed.; CRC Press: Boca Raton, FL, 2006; pp 8/20−8/29.
(42) Chen, J.; Herricks, T.; Geissler, M.; Xia, Y. *J. Am. Chem. Soc.* **2004**, *126*, 10854–10855.
(43) Grätzel, M. *Nature* **2001**, *414*, 338–344.
(44) Zhang, J.; Fang, J. *J. Am. Chem. Soc.* **2009**, *131*, 18543–18547.
(45) Kitchin, J. R.; Nørskov, J. K.; Barteau, M. A.; Chen, J. G. *J. Chem. Phys.* **2004**, *120*, 10240–10246.
(46) Mun, B. S.; Watanabe, M.; Rossi, M.; Stamenkovic, V.; Markovic, N. M.; Ross, P. N. *J. Surf. Rev. Lett.* **2006**, *13*, 697–702.
(47) Mun, B. S.; Watanabe, M.; Rossi, M.; Stamenkovic, V.; Markovic, N. M.; Ross, P. N., Jr. *J. Chem. Phys.* **2005**, *123*, 204717.
(48) Lee, S.-M.; Jun, Y.-w.; Cho, S.-N.; Cheon, J. *J. Am. Chem. Soc.* **2002**, *124*, 11244–11245.
(49) Tian, N.; Zhou, Z.-Y.; Sun, S.-G.; Ding, Y.; Wang, Z. L. *Science* **2007**, *316*, 732–735.
(50) Wang, C.; Daimon, H.; Lee, Y.; Kim, J.; Sun, S. *J. Am. Chem. Soc.* **2007**, *129*, 6974–6975.
(51) Deivaraj, T. C.; Chen, W.; Lee, J. Y. *J. Mater. Chem.* **2003**, *13*, 2555–2560.
(52) To minimize the measurement error, the diagonal of each projected image was measured and its equivalent side length was subsequently calculated based on the assumption that the projection image of each nanocrystal is exactly square.
(53) Ahrenstorf, K.; Heller, H.; Kornowski, A.; Broekaert, J. A. C.; Weller, H. *Adv. Funct. Mater.* **2008**, *18*, 3850–3856.
(54) Ahrenstorf, K.; Albrecht, O.; Heller, H.; Kornowski, A.; Gçrlitz, D.; Weller, H. *Small* **2007**, *3*, 271–274.
(55) A trace at peak (111) indicates the minor "impurity" of nanoctahedra as described in the synthesis section.
(56) Lu, W.; Fang, J.; Stokes, K. L.; Lin, J. *J. Am. Chem. Soc.* **2004**, *126*, 11798–11799.
(57) Zhang, J.; Kumbhar, A.; He, J.; Das, N. C.; Yang, K.; Wang, J.-Q.; Wang, H.; Stokes, K. L.; Fang, J. *J. Am. Chem. Soc.* **2008**, *130*, 15203–15209.
(58) Solla-Gullòn, J.; Vidal-Iglesias, F. J.; Lòpez-Cudero, A.; Garnier, E.; Feliu, J. M.; Aldaz, A. *Phys. Chem. Chem. Phys.* **2008**, *10*, 3689–3698.

DOI: 10.1021/nl903717z | *Nano Lett.* **2010,** *10,* 638-644

(59) Mayrhofer, K. J. J.; Juhart, V.; Hartl, K.; Hanzlik, M.; Arenz, M. *Angew. Chem., Int. Ed.* **2009**, *48*, 3529–3531.
(60) Clavilier, J. In *Interfacial Electrochemistry*; Wieckowski, A., Ed.; Marcel Dekker: Oxford, 1999.
(61) Solla-Gullón, J.; Vidal-Iglesias, F. J.; Herrero, E.; Feliu, J. M.; Aldaz, A. *Electrochem. Commun.* **2006**, *8*, 189–194.
(62) Solla-Gullón, J.; Rodríguez, P.; Herrero, E.; Aldaz, A.; Feliu, J. M. *Phys. Chem. Chem. Phys.* **2008**, *10*, 1359–1373.
(63) Lee, H.; Habas, S. E.; Kweskin, S.; Butcher, D.; Somorjai, G. A.; Yang, P. *Angew. Chem., Int. Ed.* **2006**, *45*, 7824–7828.
(64) Markovic, N. M.; Gasteiger, H. A.; Ross, P. N. *J. Phys. Chem.* **1996**, *100*, 6715–6721.
(65) Mayrhofer, K. J. J.; Strmcnik, D.; Blizanac, B. B.; Stamenkovic, V.; Arenz, M.; Markovic, N. M. *Electrochim. Acta* **2008**, *53*, 3181–3188.
(66) Janssen, G. J. M.; Sitters, E. F.; Pfrang, A. *J. Power Sources* **2009**, *191*, 501–509.
(67) Chhina, H.; Campbell, S.; Kesler, O. *J. Electrochem. Soc.* **2009**, *156*, B1232–B1237.
(68) Maric, R. Spray-based and CVD Processes for Synthesis of Fuel Cell Catalysts and Thin Catalyst Layers. In *PEM Fuel Cell Electrocatalysts and Catalyst Layers: Fundamentals and Applications*; Zhang, J., Ed.; Springer: London, 2008; Chapter 20, p 946.

DOI: 10.1021/nl903717z | *Nano Lett.* **2010,** *10,* 638-644